

Altered propionate metabolism contributes to tumor progression and aggressiveness

Ana P. Gomes^{1,2,8*#}, Didem Ilter^{1,2,8*}, Vivien Low^{1,2*}, Stanislav Drapela³, Tanya Schild^{1,2,10}, Edouard Mullarky^{1,4}, Julie Han^{1,2}, Ilaria Elia^{5,6}, Dorien Broekaert^{5,6}, Adam Rosenzweig^{1,2}, Michal Nagiec^{1,2}, Joana B. Nunes^{1,2}, Bethany E. Schaffer^{1,2}, Anders P. Mutvei^{1,2,9}, John M. Asara⁶, Lewis C. Cantley^{1,3}, Sarah-Maria Fendt^{5,6}, John Blenis^{1,2#}

¹ Meyer Cancer Center, Weill Cornell Medicine, New York, NY, USA.

² Department of Pharmacology, Weill Cornell Medicine, New York, NY, USA.

³ Department of Molecular Oncology, H. Lee Moffit Cancer Center & Research Institute, Tampa, FL, USA.

⁴ Department of Medicine, Weill Cornell Medicine, New York, NY, USA.

⁵ Laboratory of Cellular Metabolism and Metabolic Regulation, VIB Center for Cancer Biology, VIB, Leuven, Belgium

⁶ Laboratory of Cellular Metabolism and Metabolic Regulation, Department of Oncology, KU Leuven and Leuven Cancer Institute (LKI), Leuven, Belgium

⁷ Department of Medicine, Beth Israel Deaconess Medical Center and Harvard Medical School, Boston, MA, USA.

⁸ Present address: Department of Molecular Oncology, H. Lee Moffit Cancer Center & Research Institute, Tampa, FL, USA.

⁹ Present address: Department of Immunology, Genetics and Pathology, Uppsala University, Uppsala, Sweden

¹⁰ Present address: Department of Radiology, Memorial Sloan Kettering Cancer Center, New York, NY, USA

* Equal Contribution

Corresponding authors: ana.gomes@moffitt.org; job2064@med.cornell.edu

Introductory paragraph

The alteration of metabolic pathways is a critical strategy for cancer cells to attain the traits necessary for metastasis in disease progression. Here, we find that dysregulation of propionate metabolism produces a pro-aggressive signature in breast and lung cancer cells, increasing their metastatic potential. This occurs through the downregulation of methylmalonyl-CoA epimerase (MCEE), mediated by an ERK2-driven SP1/EGR1 transcriptional switch driven by metastatic signaling at its promoter level. The loss of MCEE results in reduced propionate-driven anaplerotic flux and the intracellular and intratumoral accumulation of methylmalonic acid (MMA), a byproduct of propionate metabolism that promotes cancer cell invasiveness. Altogether, we present a previously uncharacterized dysregulation of propionate metabolism as an important contributor to cancer and a valuable potential target in the therapeutic treatment of metastatic carcinomas.

Main text

Cancer is the second leading cause of death worldwide, and metastatic cancer accounts for the major proportion of these mortalities^{1,2}. The reprogramming of cellular metabolism for both the development of cancer and its progression to metastasis presents a ripe area of research. Far from simply existing as the process of breakdown and buildup of nutrients in the cell, cellular metabolism has become recognized as a fundamental determinant of cellular identity and function³. It is now evident that certain metabolites, known as oncometabolites, can

50 drive cancer progression and metastasis, functioning in autocrine, paracrine and endocrine
51 fashions⁴. While the influence of age, diet and lifestyle on metabolism and consequently cancer
52 progression is well established, the study of metabolic alterations that occur on the level of the
53 tumor microenvironment present exciting new avenues for targeted therapies. Recently, we
54 demonstrated how a systemic age-induced increase of a metabolite, methylmalonic acid (MMA),
55 contributes to poor cancer prognosis and increased cancer-related mortality in elderly patients⁵,
56 highlighting the importance of metabolic alterations in determining tumor progression.

57
58 Cancers, especially highly aggressive cancers, are notorious for their ability to hijack
59 physiological processes to enable their progression. To characterize the relevant metabolic
60 changes that promote cancer progression, we identified significantly altered metabolites in
61 pulmonary metastases compared to corresponding primary tumors in the 4T1 orthotopic mouse
62 model⁶ for triple negative breast cancer (TNBC) and performed a pathway enrichment analysis
63 on these metabolites (Supplementary Table 1, Fig.1a-b). It is important to note that while this
64 experiment can provide a snapshot of potential metabolites and metabolic pathways that are
65 important for TNBC metastasis, it likely does not account for the full spectrum of metabolic
66 alterations that fuel metastasis. Through this analysis, we identified processes previously known
67 to be affected in cancer progression, such as serine metabolism and ammonia recycling⁷⁻⁹.
68 Intriguingly, we also found the propionate metabolism pathway enriched in metastatic tumors, of
69 which methylmalonic acid (MMA), a systemically increased aging-induced metabolite that we
70 recently identified to contribute to metastatic aggressiveness, is a byproduct⁵ (Fig. 1c). Based
71 on these results, we hypothesized that TNBC cells may hijack propionate metabolism in order to
72 accumulate MMA, abetting a metabolic change that enhances metastatic success. To test if
73 increased MMA levels within the tumor was correlated with metastasis, we measured MMA
74 concentrations using LC-MS/MS in the primary tumors against the metastatic tumors of a 4T1
75 breast tumor mouse model. Indeed, MMA concentrations were significantly higher in
76 metastases than in primary tumors (Fig. 1d). Additionally, among clonal subpopulations isolated
77 from a single mammary tumor, MMA levels were significantly higher in a broadly metastatic 4T1
78 clone, which is able to form metastases, compared to a locally invasive 4TO7 clone, which has
79 the ability to invade out of the primary tumor but remains metastatically dormant and fails to
80 colonize secondary niches (Fig. 1e)¹⁰. These observations raised the question of whether
81 increased MMA production could be generalizable to human cancer, so we measured MMA
82 levels in a panel of human breast cell lines, including one breast epithelial cell line, three
83 receptor positive breast cancer cell lines and four TNBC metastatic-like cell lines (Fig. 1f). We
84 observed a marked increase in the metastatic TNBC cell lines compared to the receptor positive
85 breast cancer or breast epithelial cell lines, suggesting a conserved increase in MMA production
86 in human metastatic TNBCs (Extended Data Fig. 1e). Together, these observations suggest
87 that the production of MMA may be important for successful metastasis of TNBCs.

88
89 In order to establish if the increase in intracellular MMA levels was an early and
90 potentially driving event in the metastatic process, we treated MCF10A and HCC1806 cells, a
91 receptor-negative breast epithelial and primary TNBC cell line, respectively, with the metastatic
92 inducers TGF β and TNF α ¹¹. Inflammatory cytokines, particularly TGF β and TNF α , have long
93 been known to contribute to acquisition of metastatic properties, particularly through their ability

94 to induce EMT in cancer cells, as well as by their ability to promote a permissive tumor
95 microenvironment¹². Three days of TGF β /TNF α treatment was sufficient to increase MMA levels
96 in these cells, consistent with its ability to promote EMT and the acquisition of pro-aggressive
97 traits (Fig. 2a, 2b, 2d). We then set out to determine if MMA was being produced from propionyl-
98 CoA or from intermediates of the TCA cycle. Using a combination of ¹³C-labeled valine,
99 isoleucine, threonine and methionine (AA) to monitor flux through the propionate metabolism
100 pathway, or ¹³C-labeled glucose and glutamine (GG) to measure their contribution to MMA
101 production via the TCA cycle. Although we cannot exclude a significant contribution of odd chain
102 fatty acid (OCFA) catabolism, our data show that a major fraction of the increase in intracellular
103 MMA was derived from catabolism of AA through the propionate metabolic pathway (Fig. 2c).
104 To determine how MMA was being increased, we surveyed expression of the enzymes involved
105 in propionate metabolism. In MCF-10A and HCC1806 cells, TGF β /TNF α promoted a loss of
106 methylmalonyl-CoA epimerase (MCEE) expression that coincided with the loss of epithelial and
107 gain of mesenchymal markers (Fig. 2d). MCEE converts the D-isomer of methylmalonyl-CoA to
108 the L-isomer that can be acted upon downstream by methylmalonyl-CoA mutase (MUT) to
109 produce succinyl-CoA, which subsequently feeds into the TCA cycle (Fig. 1c). MCEE loss
110 results in accumulation of D-methylmalonyl CoA and consequently, increased MMA, as seen in
111 TGF β /TNF α mediated repression of MCEE (Fig. 1c, 2a-b). Additionally, we found that MCEE
112 loss correlated with the metastatic ability of 4T1 clones, with decreased expression in broadly
113 metastatic compared to locally invasive clones (Extended Data Fig. 1a). We also observed
114 decreased protein expression of MCEE in metastatic versus non-metastatic cell lines (Fig. 2e).
115 When comparing receptor negative primary cancer cells versus cells obtained from metastatic
116 TNBCs, we often observed increased propionyl CoA carboxylase (PCC) expression (Fig. 2e,
117 Extended Data Fig. 1a), although this was not induced by TGF β /TNF α during the time frame we
118 have studied. These data implicate the conversion of the D- to L-isomer of methylmalonyl-CoA
119 as the common point of disruption in propionate metabolism by TGF β /TNF α and the likely
120 source of increased MMA production during metastatic signaling. Importantly, this observation is
121 not specific to TNBCs as treatment of lung adenocarcinoma cells (A549) with TGF β /TNF α ,
122 which promotes the acquisition of metastatic properties in these types of cancer, also promoted
123 increased accumulation of MMA, which correlated with suppression of MCEE expression
124 (Extended Data Fig. 1b-c). In accordance with the importance of MCEE expression levels for
125 TNBC metastasis, analysis of publicly available databases shows that low expression of MCEE
126 in lymph node positive TNBC tracks with significantly reduced survival and poor prognosis
127 (Extended Data Fig. 1f-g). Combined, these data indicate that MCEE is the point of propionate
128 metabolism deregulation by metastatic inducers and an important metabolic regulatory node in
129 TNBCs.

130

131 Next, we sought to understand how MCEE expression is regulated by metastatic
132 signaling. Much of the metastatic process stems from alterations in gene expression driven by
133 transcriptional reprogramming^{13,14}, therefore we asked if reduced MCEE expression was the
134 result of altered transcription. In support of this idea, MCEE mRNA levels were downregulated
135 upon treatment with TGF β /TNF α (Fig. 2f-g). A marked loss of MCEE promoter activity confirmed
136 that the suppression of MCEE protein levels in MCF10A and A549 cells by TGF β /TNF α was
137 transcriptional (Fig. 2h, Extended Data Fig. 1d). Upon analysis of the MCEE promoter region,

138 we found overlapping EGR1/SP1 binding sites, which are both downstream effectors of ERK
139 (Fig. 2i). We have previously demonstrated that overlapping EGR1/SP1 binding sites can
140 function as a switch downstream of ERK2 signaling. Upon ERK2 signaling, phosphorylated
141 SP1, a positive regulator of this promoter, becomes dephosphorylated and EGR1, a negative
142 regulator of this promoter that is dramatically induced, replaces SP1 and promotes
143 transcriptional repression¹³. To determine if a similar mechanism could be at play, we used an
144 ERK2 D319N-induced model of metastatic signaling in MCF10A cells^{15,16}. As in the TGF β /TNF α
145 induced breast and lung cancer cells, we saw that ERK2 D319N expression suppressed
146 expression of MCEE compared to control cells, while markedly increasing MMA levels (Fig. 2j-
147 k). Importantly, in this ERK2 D319N-overexpressing system, MCEE promoter activity was also
148 suppressed, supporting an ERK2-driven transcriptional regulation at the overlapping EGR1/SP1
149 binding sites (Fig. 2l). Knockdown of SP1 in both MCF10A and HCC1806 cells mimicked ERK2-
150 mediated suppression of MCEE (Fig. 2m). Additionally, a phospho-mimetic mutant of SP1 was
151 able to rescue MCEE expression in ERK2-induced MCF10A cells, whereas wild-type SP1 and a
152 non-phosphorylatable form of SP1 maintained suppression, despite induction of EGR1 (Fig. 2n).
153 In accordance with this model, inhibition of ERK suppressed the ability of TGF β /TNF α to induce
154 EGR1 and SP1 dephosphorylation and concomitantly also blocked TGF β /TNF α mediated
155 repression of MCEE expression (Fig. 2o). Together, our data support a mechanism in which
156 metastatic signaling, dependent on ERK, promotes MMA production by creating an environment
157 where phosphorylated SP1, a positive regulator of MCEE expression, becomes
158 dephosphorylated and is replaced by EGR1 in the promoter region of MCEE, antagonizing
159 MCEE expression.

160
161 To support our findings highlighting the link between dysregulation of propionate
162 metabolism to metastatic progression, we utilized a genetic approach. MCEE knockdown,
163 which mimicked its suppression by metastasis inducers and resulted in increased MMA levels
164 (Extended Data Fig. 2a-b), was sufficient to regulate expression of pro-aggressive markers
165 associated with cancer progression, including loss of epithelial and gain of mesenchymal
166 markers, in MCF-10A, HCC1806 and A549 cells (Extended Data Fig. 2c). We next sought to
167 resolve whether increasing MMA through alteration of other points of the propionate metabolism
168 pathway could similarly increase metastatic aggressiveness. Toward this end, we knocked
169 down MUT in A549, MCF-10A and HCC1806 cells, which also led to increased levels of MMA
170 and, as in MCEE knockdown, pro-aggressive markers were altered (Fig. 3a-b, Extended Data
171 Fig. 3a-c). We have previously shown that MMA is sufficient to induce a pro-metastatic gene
172 expression profile⁵, and similarly, knockdown of MUT also induced a similar gene expression
173 profile with metastatic characteristics, including increased expression of *SOX4*, *TFGB1*,
174 *TGFBR1* and *TGFBR2* (Supplementary Table 2, Fig. 3c, Extended Data Fig. 3d-g). MMA levels
175 have been reported to be increased in the serum of individuals with vitamin B12 deficiency, due
176 to the requirement of vitamin B12 for MUT activity downstream of MCEE¹⁷. Indeed, depletion of
177 vitamin B12 from the media also replicated this effect, as did knockdown of *MMAB*, the gene
178 encoding the enzyme cob(I)alamin adenosyltransferase, which converts vitamin B12 to its
179 biologically active form utilized by MUT (Extended Data Fig. 4a-e). To further determine if
180 manipulation of propionate metabolism and MMA accumulation could promote cancer
181 progression in mice, we knocked down MUT in a metastatic breast cancer cell line, MDA-MB-

182 231 cells. Reduced expression of MUT in these cells increased MMA levels and increased the
183 cells' capacity to migrate and invade in transwell assays (Figure 3d-f). We then demonstrated
184 that these cells had increased ability to colonize and grow in lungs of mice following a tail-vein
185 injection (Fig 3g-h).

186
187 PCC catalyzes the carboxylation of BCAA and OCFA-derived propionyl-CoA into D-
188 methylmalonyl-CoA and therefore regulates flux through the propionate metabolic pathway and
189 the ability to generate MMA (Fig.1c). In accordance with this, overexpression of PCC resulted in
190 increased propionyl-CoA levels and consequently increased flux through the propionate
191 metabolic pathway, as demonstrated by an increase in MMA and succinate as well as other
192 TCA cycle intermediates (Extended Data Fig. 5a-f). Mirroring its effects on MMA levels,
193 overexpression of PCC in HCC1806, MCF-10A and A549 cells promoted pro-metastatic
194 markers (Extended Data Fig. 5g). While PCC overexpression did not have a significant effect on
195 the migratory ability of cells, it significantly increased invasion ability and lung colonization
196 following tail vein injection of MDA-MB231 cells (Extended Data Fig. 5h-k). Further supporting
197 the importance of PCC for the endogenous production of MMA in cancer cells, knockdown of
198 PCCA (one of the subunits of the PCC enzyme complex necessary for its function) abrogates
199 TGF β /TNF α -mediated increase in MMA levels (Fig. 4a). Importantly, knockdown of PCCA, while
200 having no effect by itself in pro-aggressive markers in non-metastatic cancer cells, was
201 sufficient to partially block TGF β /TNF α -induced pro-aggressive properties in these cells (Fig. 4b,
202 Extended Data Fig. 6a-b, 6d). However, PCCA knockdown had no effect in the induction of pro-
203 aggressive properties induced by exogenous MMA treatment (Fig. 4d, Extended Data Fig. 6c),
204 further supporting the dependence on MMA for PCC-mediated regulation of pro-aggressive
205 properties. Finally, a MDA-MB-231 cell line clone has been isolated with greatly increased
206 ability to colonize and grow in lungs, MDA-MB-231-LM2¹⁸. Interestingly, MDA-MB-231-LM2 cells
207 show an increase in MMA levels compared to its parental line (Extended Data Fig. 3h) which
208 has less ability to effectively form metastatic colonies¹⁸. Knockdown of PCC in these cells
209 dramatically suppressed their metastatic potential, affecting their expression of mesenchymal
210 markers in an MMA-dependent manner, inhibiting their ability to migrate and invade in
211 transwells assays (Fig. 4c-f), a phenomenon also observed in another cell line with high
212 metastatic potential (Hs578T; Extended Data Fig. 6e-g), and reducing their capacity to colonize
213 the lungs of mice (Fig. 4g-h). PCCA knockdown in the highly metastatic cell lines MDA-MB-231-
214 LM2 and Hs578T also affected their ability to proliferate (Extended Data Fig. 6h-i). Although we
215 cannot discard the possibility that this effect may be influenced by changes in TCA cycle
216 intermediates unrelated to MMA levels, together, our data reveal an important regulatory role of
217 PCC in the endogenous production of MMA by cancer cells and suggest that PCC might
218 constitute a valuable therapeutic target for metastatic TNBC.

219
220 We have recently reported that the metabolite MMA represents a vital link between
221 aging and the severity of cancer prognosis⁵. Now, we demonstrate that cancer cells themselves
222 are able to increase MMA levels by altering propionate metabolism in highly aggressive cancers
223 such as TNBCs, allowing them to undergo a pro-metastatic reprogramming. Through
224 transcriptional inhibition of MCEE, flux through propionate metabolism was impeded, resulting in
225 accumulation of MMA. Together, we reveal a strategy utilized by cancer cells to acquire the

226 aggressive traits and capabilities imperative to the progression of disease, centered around the
227 accumulation of an endogenous metabolic byproduct. While the dysregulation of propionate
228 metabolism to accumulate MMA within the tumor, and the revelation of its dual roles as both a
229 tumor-produced as well as an age-associated systemic oncometabolite, underscores the
230 significance of MMA in cancer, many questions remain to be elucidated. Does the MMA
231 produced by tumor cells function primarily in an autocrine fashion, or can it also be secreted to
232 act upon neighboring tumor cells and other cell types? How does MMA regulate the
233 transcriptional program that underlies metastatic ability? At this point in our venture, there is still
234 much to be uncovered about this previously disregarded metabolite. Our findings provide a
235 foundation for further research that will conceivably widen the scope of our understanding of
236 metabolic reprogramming in the tumor microenvironment, aging, and cancer.

237 **Methods**

238 Email contact for reagent and resource sharing: ana.gomes@moffitt.org and
239 job2064@med.cornell.edu

240 **Cell Lines**

241 All human breast epithelial and cancer cell lines, unless indicated otherwise, were obtained from
242 the American Type Culture Collection (ATCC). MCF-10A (ATCC: CRL-10317) cells were
243 cultured in DMEM:F12 media (Corning) supplemented with 5% horse serum (Gibco), 10 µg/mL
244 insulin (Sigma-Aldrich), 100 ng/mL cholera toxin (Sigma-Aldrich), 20 ng/mL EGF (Peprotech),
245 and 0.5 mg/mL hydrocortisone (Sigma-Aldrich). SKBR3 (ATCC: HTB-30) cells were maintained
246 in McCoy's 5a (Corning) media supplemented with 10% FBS (Sigma-Aldrich). MCF-7 (ATCC:
247 HTB-22), T47D (ATCC: HTB-133) and BT-549 (ATCC: HTB-122) cells were cultured in RPMI-
248 1640 (Corning) medium supplemented with 10% FBS and 0.01 mg/ml insulin (Sigma-Aldrich) for
249 MCF7 and T47D, and 0.001 mg/ml insulin for BT-549. A549 (ATCC: CCL-185), HCC1806
250 (ATCC: CRL-2335), BT-20 (ATCC: HTB-19), HCC38 (ATCC: CRL-2314), MDA-MB-231 (ATCC:
251 HTB-26) and MDA-MB-436 (ATCC: HTB-130) cells were cultured in RPMI-1640 medium
252 supplemented with 10% FBS. Hs578T (ATCC: HTB-126) cells were maintained in high glucose
253 DMEM (Gibco) with 0.01 mg/ml insulin and 10% FBS. MDA-MB-231-luciferase parental and
254 metastatic LM2 subclone cells, described previously¹⁸, were obtained from Dr. Massague's lab
255 and were maintained in high glucose DMEM supplemented with 10% FBS. HEK293T cells
256 were obtained from GenHunter and cultured in high glucose DMEM supplemented with 10%
257 FBS. Mouse breast cancer cell line clones 4T1, the metastatic one, and the locally invasive
258 clone 4TO7 were originally derived by Dr. F. Miller¹⁹ and obtained from Dr. William Schieman.
259 They were maintained in RPMI-1640 with 10% FBS. All cell lines were cultured at 37°C and 5%
260 CO₂ in the presence of 100 unit/ml penicillin and 100 µg/ml streptomycin (Gibco). Additionally,
261 all cell lines were maintained mycoplasma negative at all times through routine testing with
262 MycoAlert mycoplasma detection kit (Lonza).

263 **Mice**

264 4 to 6 weeks old female nu/nu athymic mice or female BALB/cOlaHsd mice were obtained from
265 Envigo. Once received, the animals were allowed to acclimate for at least 7 days before the
266 xenograft experiments. The maximum tumor size allowed by Weill Cornell Medicine institutional
267 review board is 20 mm or 2.5 cm³, or 10% of the animal's body weight, and this maximum size
268 was not exceeded. The nu/nu mice were maintained at Weill Cornell Medicine in compliance to
269 Weill Cornell Medicine Institutional Animal Care and Use Committee protocols. Mice were
270 maintained under standard husbandry conditions, group housed (5 maximum) in conventional

275 cages with unrestricted food and water access. The room was maintained at 21-23 °C, around
276 50% humidity and with a 12 hours light-dark cycle. PicoLab Rodent Diet 5053 (Labdiet, Purina)
277 containing 20% protein and 5% fat was used. Mice were monitored by staff daily to observe
278 health, maintain food and water and ensure cage cleanliness. BALB/cOlaHsd mice were
279 maintained at KU Leuven/VIB in compliance with local ethical regulations and all experiments
280 were approved by the KU Leuven ethics committee. The animals were maintained with
281 unrestricted food and water access under 14h light, 10h dark cycle at 22±2 °C and between 45-
282 70% humidity. The mice were fed Ssniff Rodent Diet containing 19% protein and 3.3% fat.
283 Experiments started when mice were 6 week old and the maximum tumor size allowed by the
284 ethics committee was not exceeded. The experiments concluded when the tumors reached 1.8
285 cm³ or got ulcerated.

286
287
288

289 **METHOD DETAILS**

290

291 **Cell Culture Treatments**

292 Cells were treated with 5 ng/ml of recombinant human TGF-β1 (PeproTech) and 5 ng/ml of
293 recombinant human TNFα (PeproTech) to induce EMT for the indicated time period up to 10
294 days. For MMA treatments, cells were treated with 5 mM MMA (Tocris) for the indicated times.
295 For vitamin B12 depletion, cells were maintained in custom media missing vitamin B12. The
296 custom media was prepared by Media Preparation Core at Memorial Sloan Kettering Cancer
297 Center.

298

299 **Targeted Metabolomics and Data Analysis**

300 Metabolites were harvested, extracted and analyzed as described before²⁰. Briefly, primary
301 tumor and lung metastases were collected, washed in ice cold blood bank saline, dried on a
302 sterile compress and snap-frozen with a liquid nitrogen cooled Biosqueezer (Biospec Products).
303 Tissues were stored at -80 °C before metabolite extraction. To extract metabolites, tissues were
304 weighed and pulverized (Cryomill, Retsch) while kept frozen with liquid nitrogen. The pulverized
305 tissues were extracted with 800 μL of 62.5% methanol containing glutaric acid as an internal
306 standard and 500 μL of precooled chloroform. At 4°C, samples were vortexed for 10 min and
307 centrifuged at max speed for 10 min to separate into phases. The upper methanol/water phase
308 was collected and evaporated using vacuum centrifugation at 4°C. A 5500 QTRAP triple
309 quadrupole mass spectrometer (AB/SCIEX) coupled to a Prominence UFLC HPLC system
310 (Shimadzu) with Amide HILIC chromatography (Waters) was used to perform targeted liquid
311 chromatography-tandem mass spectrometry (LC-MS/MS). Selected reaction monitoring (SRM)
312 mode using positive/negative ion polarity switching for steady-state polar profiling of greater
313 than 260 molecules was used for all data collection. MultiQuant v2.0 software (AB/SCIEX) was
314 used to integrate peak areas from the total ion current for each metabolite SRM transition.
315 MetaboAnalyst, an open-source software (www.metaboanalyst.ca, v4.0) was used for statistical
316 analysis. Prior to further analyses, original peak intensities were normalized to the mean of the
317 entire metabolome and log transformed (Table S1).

318

319 **Methylmalonic Acid, Propionyl-CoA and TCA cycle intermediate levels and tracing**

320 Methylmalonic acid and other polar metabolites (including propionyl-CoA, succinate, fumarate,
321 malate and oxaloacetate) were extracted from cells in culture using 80% (v/v) aqueous
322 methanol as described before for polar metabolite extraction²¹ and measured by targeted LC-
323 MS/MS using the same method as described above for targeted metabolomics. For ¹³C tracing
324 experiments, HCC1806 cells were treated with TGF-β and TNFα as described above for 24
325 hours after which the medium was changed to either glucose and glutamine free RPMI

326 containing 2 g/L [U-¹³C]glucose, 300 mg/L [U-¹³C]glutamine and 10% dialyzed serum or valine,
327 isoleucine, threonine and methionine free RPMI containing 20 mg/L [U-¹³C]valine, 50 mg/L [U-
328 ¹³C]isoleucine, 20 mg/L [U-¹³C]threonine, 15 mg/L [U-¹³C]methionine and 10% dialyzed serum
329 for an additional 48 hours. TGF- β and TNF α treatments were maintained through the course of
330 the labeling timeline. Metabolites were extracted and analyzed by LC-MS/MS as described
331 above. The original peak intensity was normalized to protein levels. Data are represented as
332 relative peak intensity as no absolute quantitation was performed.
333

334 **Gene Silencing**

335 shPCCA #1 (TRCN0000078424), shPCCA #2 (TRCN0000078427), shMMAB #1
336 (TRCN0000083905), shMMAB #2 (TRCN0000083904), shMCEE #1 (TRCN0000049481),
337 shMCEE #2 (TRCN0000049482), shMUT #1 (TRCN0000049038), shMUT #2
338 (TRCN0000049042), shSP1 #1 (TRCN0000285151), shSP1 #2 (TRCN0000274208) and shNT
339 (shGFP - TRCN0000072181) (all from Sigma Aldrich) lentiviruses were produced in HEK293T
340 cells. Each construct was co-transfected with plasmids encoding pMD2.G (Addgene plasmid
341 12259) and psPAX2 (Addgene plasmid 12260) using X-tremeGENE HP (Roche) following the
342 manufacturer's instructions. Following transfection the media on the HEK293T cells was
343 changed 24 hours later, and the media containing the virus particles were collected 48 hours
344 after the media change. Cells were transduced with the filtered virus in the presence of 8 μ g/mL
345 polybrene (Sigma-Aldrich). 24 hours after being transduced, the resistant cells were selected
346 using 2 μ g/mL puromycin (Sigma-Aldrich), and maintained with 2 μ g/mL puromycin (Sigma-
347 Aldrich) in their growth media for the duration of the experiments.
348

349 **Generation of Stable Overexpressing Cell Lines**

350 Human PCCA and PCCB open reading frame clones were obtained from the human ORFeome
351 collection (PlasmidID, Harvard Medical School) and GFP was obtained from Addgene (Addgene
352 plasmid 15301) in the Gateway compatible pDONR223 vector. These DONR vectors were then
353 recombined into the Gateway destination vector PHAGE C-TAP (a kind gift from Dr. Wade
354 Harper²²) using LR clonase II (Thermo Scientific). The virus particles for these PHAGE C-TAP
355 constructs, and the mutant SP1 and pInducer20 GFP, ERK2 D319N constructs¹³ were produced
356 in HEK293T cells and cells were transduced as described above in the gene silencing section.
357 To overexpress the PCC complex, cells were infected with equal amounts of PCCA and PCCB
358 expressing virus. To isolate the transduced cells, cells were selected with either 2 μ g/mL
359 puromycin or 300 μ g/mL G418 (Sigma-Aldrich), according to their appropriate resistance. Cells
360 stably transduced with inducible GFP or ERK2 D319N vectors were treated with 0.5 μ g/mL of
361 doxycycline to induce the expression of the transgenes for the duration of the experiment.
362

363 **Proliferation Assays**

364 MDA-MB-231 LM2 metastatic clone or Hs578T cells with knockdown of PCCA for 3 days were
365 seeded on 96-well plates. The plates were placed in the Incucyte Live Cell Imaging system and
366 kept at 37°C and 5% CO₂ for the duration of the experiment. The imaging started 4 hours after
367 seeding and images were taken every 8 hours. Proliferation of the cells over time was
368 measured as increase in confluency, which was done by image analysis using the Incucyte
369 software (v. 2021A).
370

371 **Transwell Migration and Invasion Assays**

372 Luciferase-expressing parental MDA-MB-231 cells¹⁸ with knockdown of MUT for 6 days or with
373 PCC overexpression for 6 days, or metastatic clone MDA-MB-231 LM2 cells with knockdown of
374 PCCA for 6 days, or Hs578T cells with knockdown of PCCA for 6 days were used in transwell
375 migration and invasion assays²³. Boyden chamber inserts (BD Biosciences, 8 μ m pore size)
376 were first pre-coated with 25 μ g/ μ l rat tail collagen 1 (Corning) for migration assays, while BD

377 BioCoat invasion chambers coated with growth factor reduced Matrigel was utilized for invasion
378 assays. Invasion chambers were rehydrated at 37°C according to manufacturer's instructions.
379 Assay media was made up of high-glucose DMEM (Gibco) supplemented with 250 µg/mL BSA
380 (Sigma-Aldrich), while high glucose DMEM media supplemented with 10% FBS (Sigma-Aldrich)
381 (and 0.01 mg/ insulin for Hs578T cells) was used as the chemoattractant media. 5 x 10⁴ cells in
382 250 µl of assay media were then added to the top chamber of cell culture inserts in a 24-well
383 companion plate, and incubated for 6 hours (migration assay) or 20 hours (invasion assay).
384 After incubation, cells that had migrated/invaded to the lower surface of the membrane were
385 fixed by incubating in 100% ethanol for 20 minutes, then stained with 0.2% crystal violet in 2%
386 ethanol for 2 hours.

387
388 A Nikon DS-Fi2 camera was used to capture images of crystal-violet stained cells, and images
389 were quantified using an automated macro on Fiji/ImageJ (v1.52 or v1.53n). Control samples
390 were used for settings and to set thresholds for the generation of binary images from all images.
391 These images were used to quantify the percentage area covered by stained cells for every
392 condition, using two or more technical replicates.

393

394 **Immunoblots for Total Cell Lysates**

395 Cell lysates were prepared using acid extraction with 10% TCA solution (10% trichloroacetic
396 acid, 25 mM NH₄OAc, 1 mM EDTA, 10 mM Tris·HCl pH 8.0). Precipitated proteins were
397 resolubilized in a 0.1 M Tris·HCl pH 11 solution containing 3% SDS and boiled for 10-15
398 minutes. 20 ug total protein per sample as determined with the DC Protein Assay kit II (BioRad)
399 were run on SDS-PAGE under reducing conditions. The proteins were transferred from the gels
400 to nitrocellulose membranes (GE Healthcare) electrophoretically and then the membranes were
401 blocked in TBS-based Odyssey Blocking buffer (LI-COR). Membranes were incubated with the
402 primary antibodies overnight at 4°C. The antibodies used to detect the proteins of interest were:
403 E-Cadherin (610181 - BD Biosciences, Dilution 1:1000), Fibronectin (ab2413 – Abcam, Dilution
404 1:5000), Vimentin (5741S - Cell Signaling, Dilution 1:1000), Serpine1 (612024 - BD
405 Biosciences, Dilution 1:1000), CTGF (ab6992 – Abcam, Dilution 1:1000), CXCR4 (ab124824 –
406 Abcam, Dilution 1:1000), MMP2 (4022S - Cell Signaling, Dilution 1:1000), HA (sc-7392 - Santa
407 Cruz, Dilution 1:5000), EGR1 (ab133695 – Abcam, Dilution 1:1000), SP1 pS739 (ab195733 –
408 Abcam, Dilution 1:500), SP1 (39058 – Active Motif, Dilution 1:1000), ERK1/2 (9102L – Cell
409 signaling, Dilution 1:5000), ERK1/2 pT202/pY204 (4370L - Cell Signaling, Dilution 1:2000),
410 MMP9 (3852S - Cell Signaling, Dilution 1:1000), MCEE (19499-1-AP – Proteintech, Dilution
411 1:250), MMAB (ab174831 – Abcam, Dilution 1:500), MUT (ab134956 – Abcam, Dilution 1:1000),
412 PCCA (ab187686 – Abcam, Dilution 1:1000), PCCB (HPA036940 - Sigma-Aldrich, Dilution
413 1:1000) and Actin (sc1615 - Santa Cruz, Dilution 1:10,000). The membranes were then
414 incubated with the appropriate horseradish peroxidase–conjugated (HRP) anti-rabbit (NA934-
415 Cytiva, Dilution 1:10,000), anti-mouse (NA931-Cytiva, Dilution 1:10,000), or anti-goat (AP180P-
416 Millipore, Dilution 1:10,000) immunoglobulin for 2 hours at room temperature. Amersham ECL
417 detection system (GE Healthcare) was utilized to develop the signals.

418

419 **MCEE Promoter Activity**

420 MCEE promoter activity was determined using a luciferase-based promoter construct
421 (Genecopoeia, HPRM51389). MCF-10A cells treated with TGFβ1-TNFα, or expressing GFP or
422 ERK2 D319N for 1 day were transfected with the MCEE promoter using X-tremeGENE HP
423 (Roche) in accordance with the manufacturer's protocol. The day after the transfection the
424 media was replaced, and TGFβ1-TNFα treatment or doxycycline for the expression of GFP or
425 ERK2 D319N maintained in the media. A549 cells treated with TGFβ1-TNFα were similarly
426 prepared. At day 3 of treatment or expression luciferase activity was measured using a Secrete-
427 Pair Dual Luminescence Assay Kit (Genecopoeia, LF032) according to the manufacturer's

428 instructions on an Envision plate reader (PerkinElmer). To normalize for variation between
429 transfection replicates the data are presented normalized to the secreted alkaline phosphatase
430 signal.

431

432 **Gene Expression Analysis**

433 RNA was extracted from cell lines using the PureLink RNA isolation kit (Life Technologies) and
434 DNase I (Amplification grade, Sigma-Aldrich) treatment was utilized to digest contaminating
435 DNA. Using iSCRIPT cDNA synthesis kit (BioRad) cDNA was synthesized and quantitative PCR
436 (qPCR) using SYBR green master mix (Life Technologies) was performed on a QuantStudio6
437 Real-Time PCR system (Life Technologies, software version v1.3). Beta actin and Tata Binding
438 Protein (TBP) expression were used to normalize target gene expression levels. Primer
439 sequences can be found in the Supplementary Table 3.

440

441 **Global Gene Expression Analysis (RNA-sequencing)**

442 Total RNA was extracted from A549 cells with MUT knockdown for 3 days as described above.
443 The extracted RNA was sent to Active Motif for further processing and RNA-seq analysis.
444 Briefly, RNA quality was assessed by BioAnalyzer, and the RIN values for all samples were
445 10.0. Directional Poly-A RNA-seq libraries were prepared and sequenced as PE42 (42-bp
446 paired-end reads) on Illumina NextSeq 500 to a depth of 34.0–49.0M read pairs. The “TopHat”
447 algorithm v2.1.0 (Bowtie v2.2.6.0) was used to align the reads to the hg38 genome which was
448 obtained from iGenomes
449 (https://support.illumina.com/sequencing/sequencing_software/igenome.html). The alignments
450 (31.3 –46.2M aligned pairs) in the BAM files were further analyzed using the Cufflinks suite of
451 programs v2.2.1 (running consecutively: Cufflinks (2.2.1.Linux_x86_64) → Cuffcompare (v2.2.1)
452 → Cuffdiff (v2.2.2). Cufflinks was run using the hg38-genes as a reference database. The
453 cufflinks outputs were compared using cuffdiff. The accession number for the raw sequencing
454 data reported in this paper is GEO: GSE161108. Gene set enrichment using GSEA software^{24,25}
455 (v.4.0.3) was performed on genes that were significantly changed ≥ 1.5 fold. “Classic”
456 enrichment statistics and “ratio of classes” metrics were used for analysis. Number of
457 permutations were set to 1000 as suggested, and “gene set” was used as permutation type.
458 Gene Ontology (GO)-Biological Processes (BP) gene set database from the Molecular
459 Signatures Database (MSigDB) collection v6.2 was utilized.

460

461 **Lung Colonization in Mice**

462 100,000 cells in 100 μ L PBS—luciferase-expressing parental MDA-MB-231 cells¹⁸ with
463 knockdown of MUT for 6 days or with PCC overexpression for 6 days, or metastatic MDA-MB-
464 231 LM2 clone with knockdown of PCCA for 6 days—were injected into the tail veins of 7 week
465 old female nu/nu athymic mice. For each experimental group 7-10 mice were used. Lung
466 colonization was evaluated as described before^{18,26} by utilizing IVIS Spectrum CT Pre-Clinical In
467 Vivo Imaging System (Perkin-Elmer) to monitor the metastases. To determine lung colonization,
468 the luminescence was measured and quantified 6 weeks after the injections using the Living
469 Image Software (v4.5, Perkin-Elmer). All animal studies followed the guidelines of and were
470 approved by the Weill Cornell Medicine Institutional Animal Care and Use Committee.

471

472 **4T1 Syngeneic Orthotopic Tumor Mouse Model**

473 Six-week-old female BALB/c mice were inoculated with 1×10^6 4T1 cells in a volume of 50 μ l
474 PBS in the mammary fat pad. After four days, a primary tumor nodule was already established.
475 Mice were sacrificed 21 days after cancer cell injection with an overdose of Dolethal (140
476 mg/kg, 2.8 μ l per gram of animal weight of a 50 mg/ml solution). The animal study complies with
477 ethical regulations and was approved by the KU Leuven ethics committee.

478

479 **Statistical Analysis**

480 Data analyses were performed using Microsoft Excel 2013 or 365 and GraphPad Prism 7 or 9.
481 A two-tailed paired Student's t test was used to determine significance when two conditions
482 were compared; for experiments with more than two conditions a one-way or two-way ANOVA
483 as indicated in figure legends was used to determine significance. In both types of statistical
484 analyses values of $p < 0.05$ were considered significant. Data are represented as the mean \pm
485 SEM (standard error of the mean) of individual data points, and the mean \pm SEM of at least
486 three independent experiments performed. Number of replicates and animals are reported in the
487 figure legends. For all experiments similar variances between groups were observed. Normal
488 distribution of samples was not determined. In the GSEA analysis FDR corrected p values are
489 used to determine significance.

490

491 **Data Availability**

492

493 Source data information for the metabolomics experiment can be found on Supplementary
494 Table 1. RNA sequencing data that support the findings of this study have been deposited in the
495 Gene Expression Omnibus (GEO) under the accession code GSE161108, as well as summary
496 information in Supplementary Table 2. The raw data supporting each figure and the raw images
497 for the western blots can be found in the corresponding Source Data files.

498

499 For RNA-seq analysis, the hg38 reference genome database was obtained from iGenomes
500 (https://support.illumina.com/sequencing/sequencing_software/igenome.html) and the GSEA
501 analysis was done with gene sets derived from the GO biological processes gene sets in the
502 Molecular Signatures Database (MSigDB) collection v6.2, which can be accessed through
503 <https://www.gsea-msigdb.org/gsea/msigdb/index.jsp>.

504

505 **Code Availability**

506

507 Fiji/ImageJ macro for automation of quantification of transwell migration and invasion assays is
508 not a standalone code but is available from the corresponding authors upon reasonable request.

509

510 **Acknowledgments**

511

512 We are grateful to members of the Blenis and Cantley Laboratories for critical input on this
513 project. We are also thankful to Dr. William Schiemann for the 4T1 clones and Melanie Planque
514 for experimental assistance. The Gomes Lab is supported by a Pathway to Independence
515 Award to A.P.G. from NCI (R00CA218686), a New Innovator Award from OD/NIH (DP2
516 AG0776980) to A.P.G., the American Lung Association, the Florida Health Department
517 Bankhead-Coley Research Program, the Florida Breast Cancer Foundation, and the George
518 Edgecomb Society of Moffitt Cancer Center. T.S. is supported by the NIH F31 pre-doctoral
519 fellowship F31CA220750. This research was supported by the NIH grant R01CA46595 and a
520 research agreement with Highline Therapeutics to J.B. S.M.F. is funded by the European
521 Research Council under the ERC Consolidator Grant Agreement number 711486 –
522 MetaRegulation, FWO research grants and projects, KU Leuven Methusalem Co-funding and
523 Fonds Baillet Latour.

524

525

526 **Author Contributions Statement**

527
528 A.P.G and J.B. conceived the project. A.P.G. and D.I. performed all the molecular biology
529 experiments, the EMT-related experiments, the invasion and migration experiments, prepared
530 the RNA for RNA-seq experiments and assisted on all other experiments. V.L. and T.S.
531 performed all the mouse experiments and assisted on all other experiments. S.D. assisted with
532 the MCEE analysis in patient samples and performed the proliferation assays. A.P.M. and B.S.
533 quantified the migration and invasion experiments. A.R. produced the viral particles, generated
534 the genetically modified cell lines, performed the qPCR analysis of MCEE and assisted with
535 metabolite extractions and MMA measurements. J.H. generated the constructs and assisted in
536 the EMT-related experiments. D.B. and I.E. collected the tumor and metastases tissues and
537 prepared the samples for metabolomic analysis. T.S. and E.M. prepared and analyzed the C13
538 tracing analysis and assisted on all other metabolite measurements. M.N. and J.N. optimized
539 the ERK2-D319N mutant. J.A. performed the metabolomics analysis. A.P.G., J.A., L.C.C.,
540 S.M.F. and J.B. supervised the project. A.P.G., D.I., V.L., A.M., B.S., E.M. and J.B. analyzed the
541 data. The manuscript was written by A.P.G., V.L. and J.B., and edited by D.I., T.S., I.E, B.S. and
542 S.M.F. All authors discussed the results and approved the manuscript.

543

544 **Competing Interests Statement**

545

546 S.M.F. has received funding from Bayer, Merck and BlackBelt Therapeutics and has consulted
547 for Fund+. L.C.C. owns equity in, receives compensation from, and serves on the Board of
548 Directors and Scientific Advisory Board of Agios Pharmaceuticals and Petra Pharma
549 Corporation. No potential conflicts of interest were disclosed by the other authors.

550

551 **Figure Legends**

552

553 **Fig. 1: Methylmalonic Acid is upregulated in breast cancer metastasis.**

554 **a, b**, Heat map (**a**) and metabolic pathway enrichment analysis (**b**) of the statistically
555 significantly altered metabolites ($FDR \leq 0.05$) in 4T1 primary tumors and pulmonary metastases
556 ($n=4$ biologically independent samples). **c**, Schematic representation of propionate metabolism.
557 **d**, Methylmalonic acid (MMA) levels in 4T1 primary tumors and pulmonary metastases ($n=4$,
558 two-tailed t -test). **e**, MMA levels in 4T1 (broadly metastatic) and 4TO7 (locally invasive) clones
559 with different metastatic potential derived from a single primary tumor ($n=5$ biologically
560 independent samples, two-tailed t -test). **f**, MMA levels in breast epithelial and breast cancer cell
561 lines ($n=5$ biologically independent samples). All values are expressed as mean \pm SEM.

562

563 **Fig. 2: Metastatic signaling leads to MMA production through regulation of MCEE. a, b,**

564 MMA levels in MCF-10A (**a**) and HCC1806 (**b**) cells treated with $TGF\beta + TNF\alpha$ for 3 days ($n=4$
565 biologically independent samples, two-tailed t -test). **c**, Fractions of labeled intracellular MMA
566 derived from glucose + glutamine (GG) or valine + isoleucine + threonine + methionine (AA) in
567 HCC1806 cells treated with $TGF\beta + TNF\alpha$ for 3 days ($n=6$ biologically independent samples,
568 two-way ANOVA with Sidak's multiple comparison test). **d, e**, Propionate metabolism-related
569 enzyme levels evaluated by immunoblots in MCF-10A and HCC1806 cells treated with $TGF\beta +$
570 $TNF\alpha$ for 3 days (**d**), and in non-metastatic and metastatic triple negative breast cancer human

571 cell lines (**e**); representative images (n=4 biologically independent samples). **f, g**, MCEE mRNA
572 levels evaluated by qPCR in MCF-10A (**f**) and HCC1806 (**g**) cells treated with TGFβ + TNFα for
573 3 days (n=4 biologically independent samples, two-tailed *t*-test). **h**, MCEE-luciferase promoter
574 activity in MCF-10A cells treated with TGFβ + TNFα for 3 days (n=4 biologically independent
575 samples, two-tailed *t*-test). **i**, Schematic representation of SP1 and EGR1 binding sites in MCEE
576 promoter. **j**, Propionate metabolism-related enzyme levels evaluated by immunoblots in MCF-
577 10A cells expressing the metastatic-inducer ERK2 D319N mutant for 3 days; representative
578 images (n=4 biologically independent samples). **k**, MMA levels in MCF-10A cells expressing the
579 metastatic-inducer ERK2 D319N mutant for 3 days (n=4 biologically independent samples, two-
580 tailed *t*-test). **l**, MCEE-luciferase promoter activity in MCF-10A cells expressing the metastatic-
581 inducer ERK2 D319N mutant for 3 days (n=4 biologically independent samples, two-tailed *t*-
582 test). **m, n**, MCEE protein levels evaluated by immunoblot in MCF-10A and HCC1806 cells with
583 SP1 knockdown for 3 days (**m**) and in MCF-10A cells expressing the ERK2 D319N mutant and
584 either SP1 wild-type or the SP1 T453/T739 phosphorylation site mutants (S to A phospho-
585 defective mutant; S to E, phospho-mimetic mutant) for 3 days (**n**); representative images (n=4
586 biologically independent samples). **o**, MCEE, EGR1 and phospho SP1 protein levels evaluated
587 by immunoblot in HCC1806 treated with TGFβ + TNFα or TGFβ + TNFα + MEK inhibitor for 3
588 days; representative images (n=4 biologically independent samples). All values are expressed
589 as mean ± SEM.

590
591 **Fig. 3: Intracellular MMA production promotes EMT and aggressive properties.** **a, b**, MMA
592 levels (one-way ANOVA with Tukey's multiple comparison test) (**a**) and immunoblots for EMT
593 and aggressiveness markers (**b**) in HCC1806 cells with MUT knockdown for 3 days;
594 representative images (n=4 biologically independent samples). **c**, Functional annotation
595 clustering analysis of mRNAs that changed >1.5-fold when evaluated by RNA sequencing in
596 A549 cells with MUT knockdown for 3 days (n=3 biologically independent samples). **d**, MMA
597 levels in MDA-MB-231-luciferase parental cells with MUT knockdown for 3 days (n=4
598 biologically independent samples, one-way ANOVA with Tukey's multiple comparison test). **e**,
599 **f**, Transwell migration (**e**) or invasion (**f**) assays of MDA-MB-231-luciferase parental cells with
600 knockdown of MUT for 6 days (n=4 biologically independent samples, one-way ANOVA with
601 Tukey's multiple comparison test). **g, h**, Lung colonization assay of MDA-MB-231-luciferase
602 parental cells injected after 6 days of MUT knockdown imaged at 6 weeks; representative
603 images (**g**) and quantification (**h**) (n=8 biologically independent animals for shNT and shMUT#2
604 and n=7 for shMUT#1, one-way ANOVA with Tukey's multiple comparison test). All values are
605 expressed as mean ± SEM.

606
607 **Fig. 4: PCC regulates MMA levels and determines pro-aggressive properties.** **a**, MMA
608 levels in MCF-10A cells with PCCA knockdown and treated with TGFβ + TNFα for 3 days (n=4
609 biologically independent samples, two-way ANOVA with Sidak's multiple comparison test). **b**,
610 EMT-related proteins evaluated by immunoblots in MCF-10A cells with PCCA knockdown and
611 treated with TGFβ + TNFα for 5 days; representative images (n=4 biologically independent
612 samples). **c**, MMA levels in MDA-MB-231-LM2 cells with PCCA knockdown for 5 days (n=4
613 biologically independent samples, one-way ANOVA with Tukey's multiple comparison test). **d**,
614 Mesenchymal protein levels evaluated by immunoblots in MDA-MB-231-LM2 cells with PCCA

615 knockdown and treated with 5 mM MMA for 5 days; representative images (n=4 biologically
616 independent samples). **e, f**, Transwell migration (**e**) or invasion (**f**) assays of MDA-MB-231-
617 luciferase LM2 cells with knockdown of PCCA for 6 days (n=4 biologically independent samples,
618 one-way ANOVA with Tukey's multiple comparison test). **g, h**, Lung colonization assay of
619 MDA-MB-231-luciferase LM2 cells with knockdown of PCCA for 6 days; representative images
620 (**g**) and quantification (**h**) (n=10 biologically independent animals, one-way ANOVA with Tukey's
621 multiple comparison test). All values are expressed as mean \pm SEM.

622

623 References

624

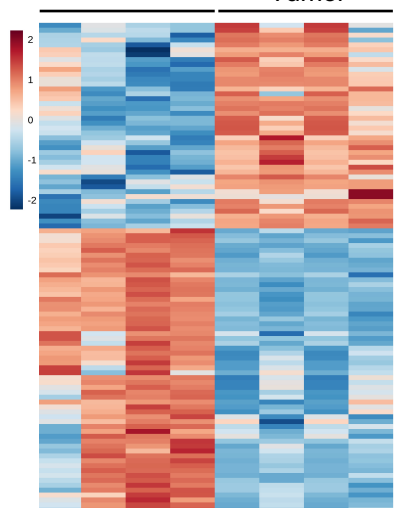
- 625 1 Dillekas, H., Rogers, M. S. & Straume, O. Are 90% of deaths from cancer caused by
626 metastases? *Cancer Med* **8**, 5574-5576, doi:10.1002/cam4.2474 (2019).
- 627 2 Mortality, G. B. D. & Causes of Death, C. Global, regional, and national life expectancy,
628 all-cause mortality, and cause-specific mortality for 249 causes of death, 1980-2015: a
629 systematic analysis for the Global Burden of Disease Study 2015. *Lancet* **388**, 1459-
630 1544, doi:10.1016/S0140-6736(16)31012-1 (2016).
- 631 3 DeBerardinis, R. J. & Chandel, N. S. Fundamentals of cancer metabolism. *Sci Adv* **2**,
632 e1600200, doi:10.1126/sciadv.1600200 (2016).
- 633 4 Corrado, M., Scorrano, L. & Campello, S. Changing perspective on oncometabolites:
634 from metabolic signature of cancer to tumorigenic and immunosuppressive agents.
635 *Oncotarget* **7**, 46692-46706, doi:10.18632/oncotarget.8727 (2016).
- 636 5 Gomes, A. P. *et al.* Age-induced accumulation of methylmalonic acid promotes tumour
637 progression. *Nature*, doi:10.1038/s41586-020-2630-0 (2020).
- 638 6 Tao, K., Fang, M., Alroy, J. & Sahagian, G. G. Imagable 4T1 model for the study of late
639 stage breast cancer. *BMC Cancer* **8**, 228, doi:10.1186/1471-2407-8-228 (2008).
- 640 7 Rinaldi, G. *et al.* In Vivo Evidence for Serine Biosynthesis-Defined Sensitivity of Lung
641 Metastasis, but Not of Primary Breast Tumors, to mTORC1 Inhibition. *Mol Cell* **81**, 386-
642 397 e387, doi:10.1016/j.molcel.2020.11.027 (2021).
- 643 8 Ngo, B. *et al.* Limited Environmental Serine and Glycine Confer Brain Metastasis
644 Sensitivity to PHGDH Inhibition. *Cancer Discov* **10**, 1352-1373, doi:10.1158/2159-
645 8290.CD-19-1228 (2020).
- 646 9 Spinelli, J. B. *et al.* Metabolic recycling of ammonia via glutamate dehydrogenase
647 supports breast cancer biomass. *Science* **358**, 941-946, doi:10.1126/science.aam9305
648 (2017).
- 649 10 Aslakson, C. J. & Miller, F. R. Selective events in the metastatic process defined by
650 analysis of the sequential dissemination of subpopulations of a mouse mammary tumor.
651 *Cancer Res* **52**, 1399-1405 (1992).
- 652 11 Padua, D. & Massague, J. Roles of TGFbeta in metastasis. *Cell Res* **19**, 89-102,
653 doi:10.1038/cr.2008.316 (2009).
- 654 12 Liu, J., Lin, P. C. & Zhou, B. P. Inflammation fuels tumor progress and metastasis. *Curr*
655 *Pharm Des* **21**, 3032-3040, doi:10.2174/1381612821666150514105741 (2015).
- 656 13 Gomes, A. P. *et al.* Dynamic Incorporation of Histone H3 Variants into Chromatin Is
657 Essential for Acquisition of Aggressive Traits and Metastatic Colonization. *Cancer Cell*
658 **36**, 402-417 e413, doi:10.1016/j.ccell.2019.08.006 (2019).

- 659 14 Iwamoto, T. *et al.* Distinct gene expression profiles between primary breast cancers and
660 brain metastases from pair-matched samples. *Sci Rep* **9**, 13343, doi:10.1038/s41598-019-
661 50099-y (2019).
- 662 15 Shin, S., Dimitri, C. A., Yoon, S. O., Dowdle, W. & Blenis, J. ERK2 but not ERK1
663 induces epithelial-to-mesenchymal transformation via DEF motif-dependent signaling
664 events. *Mol Cell* **38**, 114-127, doi:10.1016/j.molcel.2010.02.020 (2010).
- 665 16 Shin, S. *et al.* ERK2 regulates epithelial-to-mesenchymal plasticity through DOCK10-
666 dependent Rac1/FoxO1 activation. *Proc Natl Acad Sci U S A* **116**, 2967-2976,
667 doi:10.1073/pnas.1811923116 (2019).
- 668 17 Vashi, P., Edwin, P., Popiel, B., Lammersfeld, C. & Gupta, D. Methylmalonic Acid and
669 Homocysteine as Indicators of Vitamin B-12 Deficiency in Cancer. *PLoS One* **11**,
670 e0147843, doi:10.1371/journal.pone.0147843 (2016).
- 671 18 Minn, A. J. *et al.* Genes that mediate breast cancer metastasis to lung. *Nature* **436**, 518-
672 524, doi:10.1038/nature03799 (2005).
- 673 19 Miller, F. R., Miller, B. E. & Heppner, G. H. Characterization of metastatic heterogeneity
674 among subpopulations of a single mouse mammary tumor: heterogeneity in phenotypic
675 stability. *Invasion Metastasis* **3**, 22-31 (1983).
- 676 20 Broekaert, D. & Fendt, S. M. Measuring In Vivo Tissue Metabolism Using (13)C
677 Glucose Infusions in Mice. *Methods Mol Biol* **1862**, 67-82, doi:10.1007/978-1-4939-
678 8769-6_5 (2019).
- 679 21 Yuan, M., Breitkopf, S. B., Yang, X. & Asara, J. M. A positive/negative ion-switching,
680 targeted mass spectrometry-based metabolomics platform for bodily fluids, cells, and
681 fresh and fixed tissue. *Nat Protoc* **7**, 872-881, doi:10.1038/nprot.2012.024 (2012).
- 682 22 Huttlin, E. L. *et al.* The BioPlex Network: A Systematic Exploration of the Human
683 Interactome. *Cell* **162**, 425-440, doi:10.1016/j.cell.2015.06.043 (2015).
- 684 23 Bos, P. D. *et al.* Genes that mediate breast cancer metastasis to the brain. *Nature* **459**,
685 1005-1009, doi:10.1038/nature08021 (2009).
- 686 24 Mootha, V. K. *et al.* PGC-1alpha-responsive genes involved in oxidative phosphorylation
687 are coordinately downregulated in human diabetes. *Nat Genet* **34**, 267-273,
688 doi:10.1038/ng1180 (2003).
- 689 25 Subramanian, A. *et al.* Gene set enrichment analysis: a knowledge-based approach for
690 interpreting genome-wide expression profiles. *Proc Natl Acad Sci U S A* **102**, 15545-
691 15550, doi:10.1073/pnas.0506580102 (2005).
- 692 26 Oskarsson, T. *et al.* Breast cancer cells produce tenascin C as a metastatic niche
693 component to colonize the lungs. *Nat Med* **17**, 867-874, doi:10.1038/nm.2379 (2011).
- 694
695
696
697
698
699

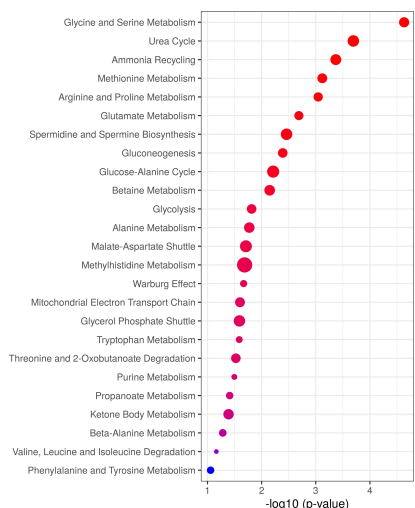
Figure 1

a

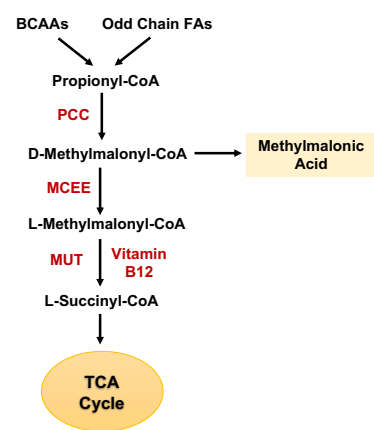
Metastasis Primary Tumor



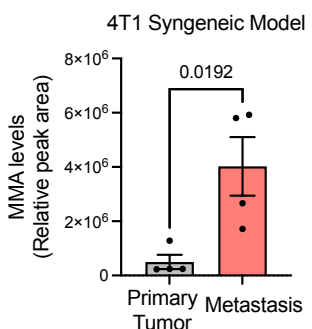
b



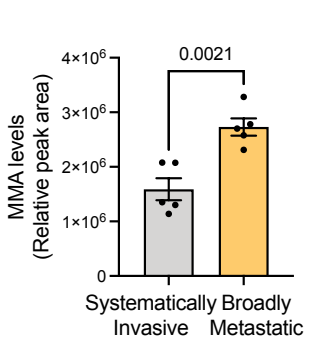
c



d



e



f

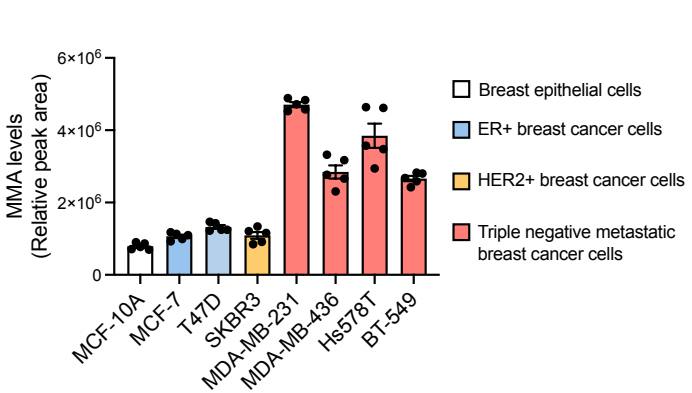


Figure 2

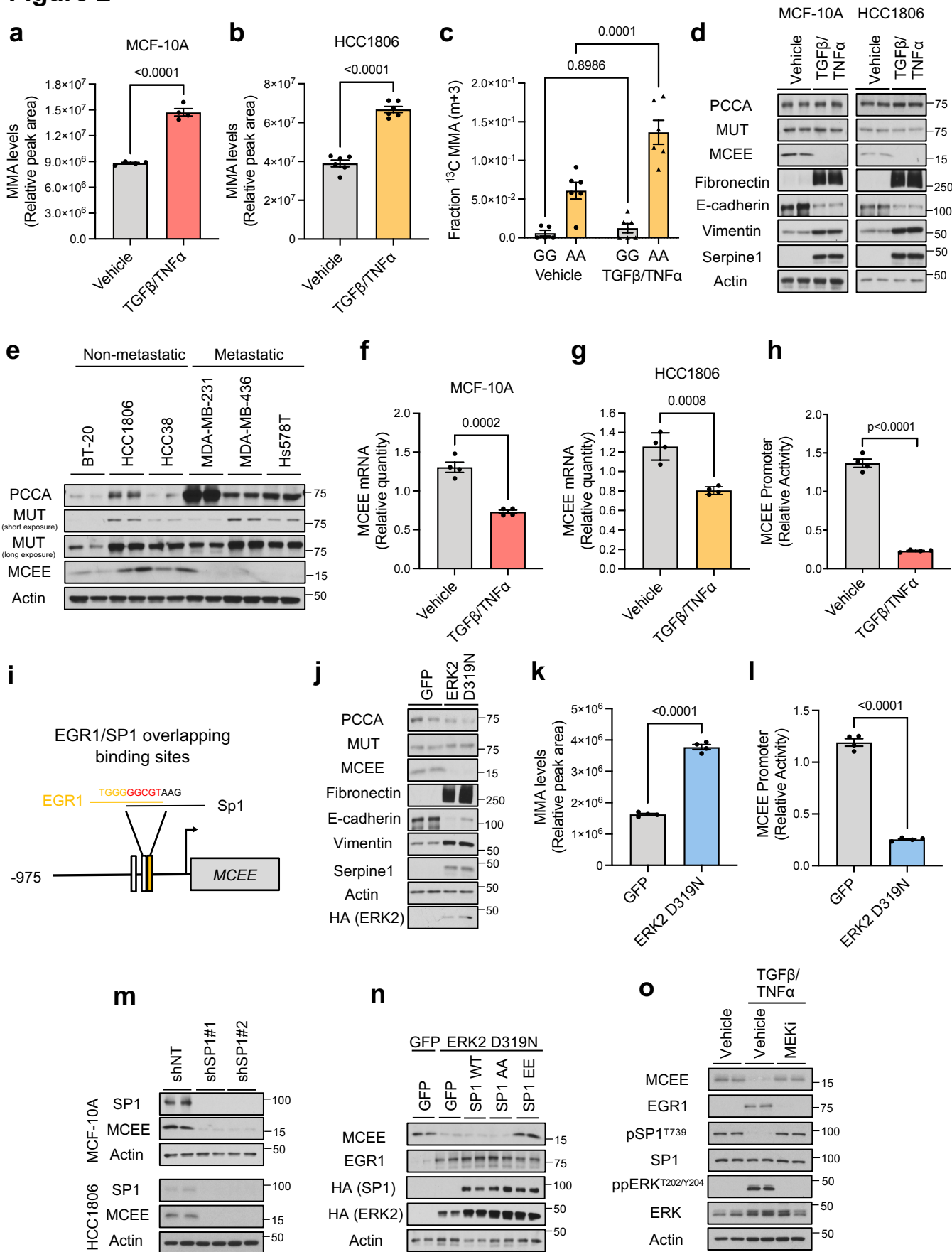


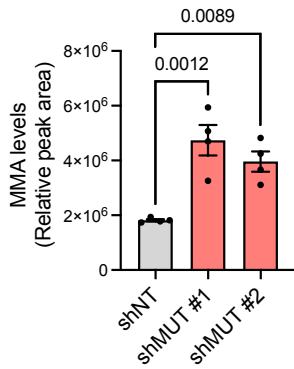
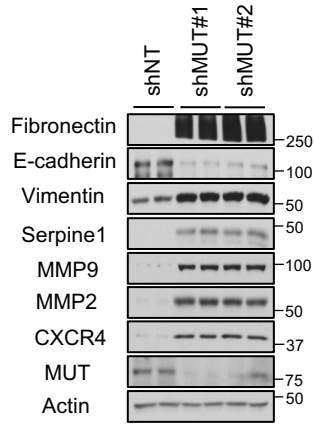
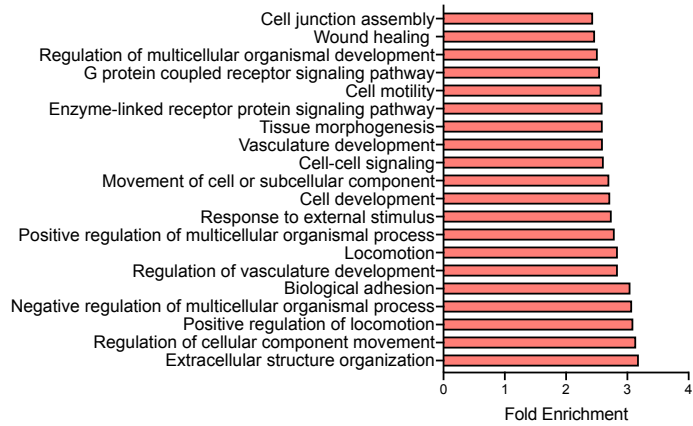
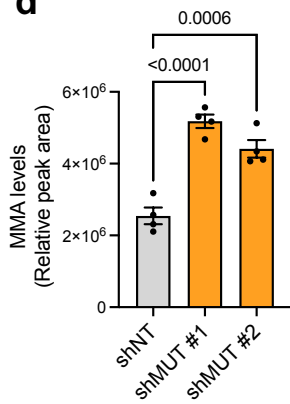
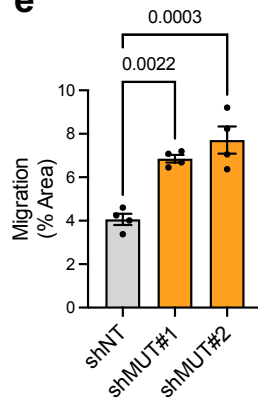
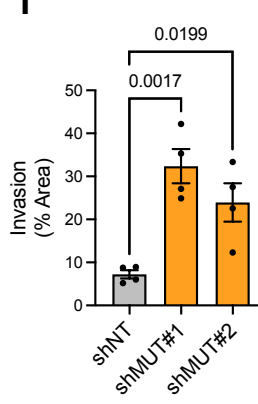
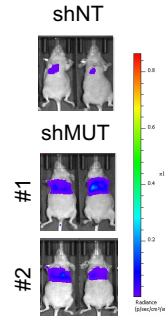
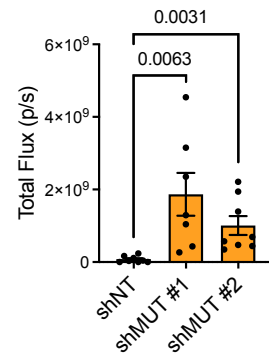
Figure 3**a****b****c****d****e****f****g****h**

Figure 4

